www.ietdl.org

Published in IET Power Electronics
Received on 27th May 2011
doi: 10.1049/iet-pel.2011.0371

ISSN 1755-4535

Real-time implementation of adaptive fuzzy hysteresis-band current control technique for shunt active power filter

Y. Suresh A.K. Panda M. Suresh

Department of Electrical Engineering, NIT Rourkela, India
E-mail: ysuresh.ee@gmail.com

Abstract: Optimising the performance of power system networks using conventional methods is quite difficult because of the complex nature of systems that are highly non-linear and non-stationary. In this study a hybrid adaptive fuzzy hysteresis current controller for shunt active power filter (SAPF) is proposed. The conventional adaptive hysteresis concept is hybridised with fuzzy logic controller (FLC), which facilitates discarding of uncertainty in the system. In fact, conventional proportional-integral (PI) controllers for shunt active filter are based on a linearised model that fails to react under transient events. On the other side, FLC has widened its applicability to many engineering fields and offers satisfactory results for a wide variety of operating conditions. It helps in fulfilling the need for perfection, such as stability and robustness for every system. All this motivated to adopt FLC for SAPF applications. By incorporating an adaptive fuzzy hysteresis band, active power filter (APF) gains outstanding compensation ability under steady-state and transient conditions. To validate the proposed approach, the system is implemented on a real-time digital simulator and adequate results are reported for its verification.

1 Introduction

Electrical power is perhaps the most essential raw material used by commerce and industry today. It is an unusual commodity because it is required as a continuous flow. From the consumers' point of view continuity of supply is an important aspect but in the present day, owing to the presence of non-linear loads continuity seems to be distractive and it is all because of power quality problems. It is important to realise that the electrical load is not static. Differences in duty cycle of equipment and variations in working pattern contribute to a constantly changing load pattern. This results in generating harmonics. Today, harmonics is a buzz word heard from electrical utilities to customers. Although harmonic voltages and currents are, by themselves, imperceptible, the physical phenomena that accompany them are perceivable [1]. The adverse effects of harmonics in electrical power systems are very real and failures related to voltage and current harmonics very often occur without warning. To reduce this harmonic propagation, active and passive filters are introduced. However, passive filters have demerits like fixed compensation characteristics [2], parallel and series resonance with source voltage harmonics and filtering characteristics strongly affected by source impedance. In addition, they are also bulky in nature and they lose their effective performance with passage of time. Owing to these reasons active filters have been proposed as a solution to passive filter problems. Interesting features of active filters are that they are smaller in size and capable of attenuating the harmonic currents in power systems by injecting equal but opposite compensating currents [3–5]. In spite of these features, successful control of active filters requires an accurate current reference that results in exact compensation and it became our key objective to develop an appropriate controller for APF. However, this article deals completely with controller diagnosis. On the other hand, to achieve significant compensation with fast control action, hysteresis controllers are used. In fact, among the various PWM techniques, the hysteresis-band current control PWM method is popularly used because of its simplicity of implementation [6]. Besides fast response current loop and inherent-peak current limiting capability, the technique does not need any information about the system parameters. In spite of this merit, current control with fixed hysteresis band has the disadvantage that the PWM frequency varies within a band because peak-to-peak current ripple is required to control all points of the fundamental wave. Indeed, this results in increasing the switching losses in the system. To avoid these limitations an adaptive hysteresis controller is developed by the author [7]. An attractive feature of the technique is; that the band can be programmed as a function of the load and the supply parameters to optimise the PWM performance. Performing such actions results in a drastic reduction of switching loss in the system. An in-depth assessment of the control technique can be found in the above reference. It is noted that, the authors had introduced the adaptive hysteresis current control for

controlling the current ripples in interior permanent magnet (IPM) machines and synchronous motor drives. In this article, this technique is adopted in three-phase four-wire shunt active filter. The research works [8, 9] suggest that the authors have developed a controller for shunt active power filter (SAPF), which is suitable for a linearised model. However, herein, the technique is well presented with both PI and fuzzy controllers, which give satisfactory results for a wide variety of operating conditions. By incorporating adaptive hysteresis with fuzzy controller, the APF gains additional capability to track the exact reference current and operate with adjustable modulating frequency band. Therefore by implementing such a technique, the APF provides excellent harmonic compensation. To verify the proposed approach, real-time verification has been performed with a real-time digital simulator (RTDS). The results demonstrate that the proposed fuzzy approach outperforms the conventional method in terms of convergence rate and harmonic compensation.

The rest of the paper is organised as follows: the active filter topology and control strategy are briefly described in Section 2. The adaptive hysteresis technique is demonstrated in Section 3. Performance of the adaptive hysteresis technique with the PI controller is discussed in Section 4 and the proposed adaptive fuzzy hysteresis controller is discussed in Section 5. RTDSs are demonstrated in Section 6. Finally, the conclusions are given in Section 7.

2 System configuration

2.1 Description of power system

The inverter topology is presented as an active filter for a harmonic isolator in the power network and the arrangement is shown in Fig. 1. The system is configured with a 50 Hz supply with a three-phase four-wire system. The APF is connected parallel to the system at the point of common coupling (PCC). Thus, it acts as a voltage source and is capable of blocking harmonic current that flows from the non-linear loads. The proposed structure is adopted with an i_d–i_q strategy. This is demonstrated briefly in the subsequent sections.

To compensate effectively, the APF design is an important criterion. In brief, for perfect compensation, the controller must be capable of achieving the following requirements: (i) extract and inject load harmonic currents, (ii) maintain a constant DC-link voltage and (iii) avoid absorbing or generating reactive power with fundamental frequency components. Herein, the active filter control algorithm is implemented to compensate for both harmonics and reactive power absorbed by the contaminated load. Besides, to attain the compensation currents, filter behaviour is analysed. The power analysis can be done considering the inverter as a sinusoidal voltage source in parallel to the contaminated load. As a matter of fact, this voltage source cannot deliver active power in the long term; this issue has been taken into account for control analysis.

The interaction between two voltage sources, interfaced by line impedance (under steady state), is governed by the geometrical relation. From Fig. 1*b* the general expression of load current can be written as

$$i_{\mathrm{L}}(t) = \sum_{n=1}^{\infty} (I_{\mathrm{Lan}} \times \sin(n\omega t + \theta_{\mathrm{Lan}})) \tag{1}$$

This load current is decomposed into three components specifically, active and reactive at fundamental frequency and the entire harmonic component, that is

$$i_{\mathrm{L}}(t) = I_{\mathrm{La1}}\cos\theta_{\mathrm{La1}} \times \sin\omega t + I_{\mathrm{La1}}\sin\theta_{\mathrm{La1}} \times \cos\omega t + \sum_{n=2}^{\infty} (I_{\mathrm{Lan}} \times \sin(n\omega t + \theta_{\mathrm{Lan}})) \tag{2}$$

$$i_{\mathrm{L}}(t) = i_{\mathrm{La'actif}}(t) + i_{\mathrm{La'reactif}}(t) + \times i_{\mathrm{Lah}}(t) \tag{3}$$

The compensation current that the filter should produce is

$$i_{\mathrm{c}} = (-i_{\mathrm{La'reacitve}}(t) + i_{\mathrm{Lah}}(t)) \tag{4}$$

Thus, the filter should achieve this compensation, through finite control action. Extraction of compensation currents is demonstrated in the next section.

2.2 Harmonic current extraction with i_d–i_q strategy

In this paper, i_d–i_q strategy is followed for perfect compensation [10]. This strategy is demonstrated in Fig. 2*a*.

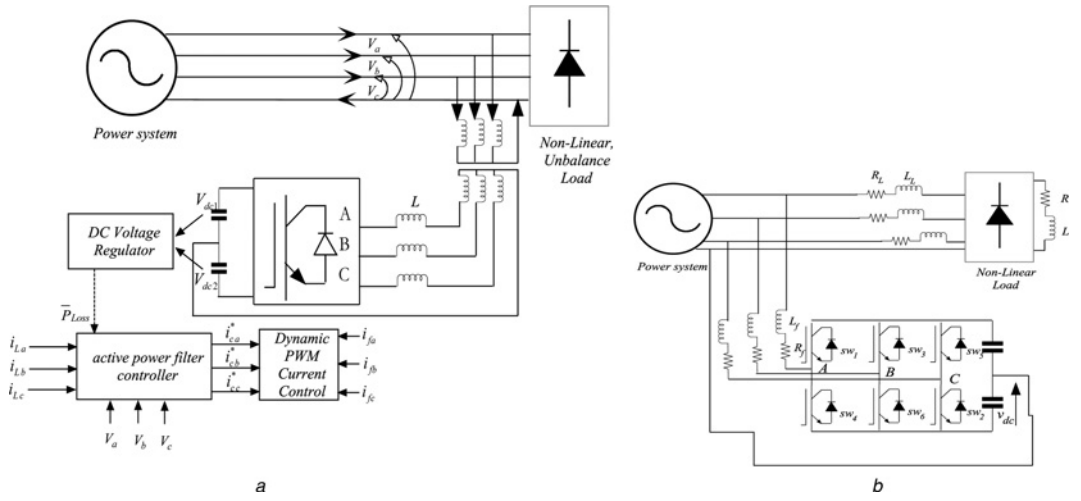

Fig. 1 *Inverter topology as active filter for harmonic isolator in power network*

a Details of active power filter
b Simplified system under steady state

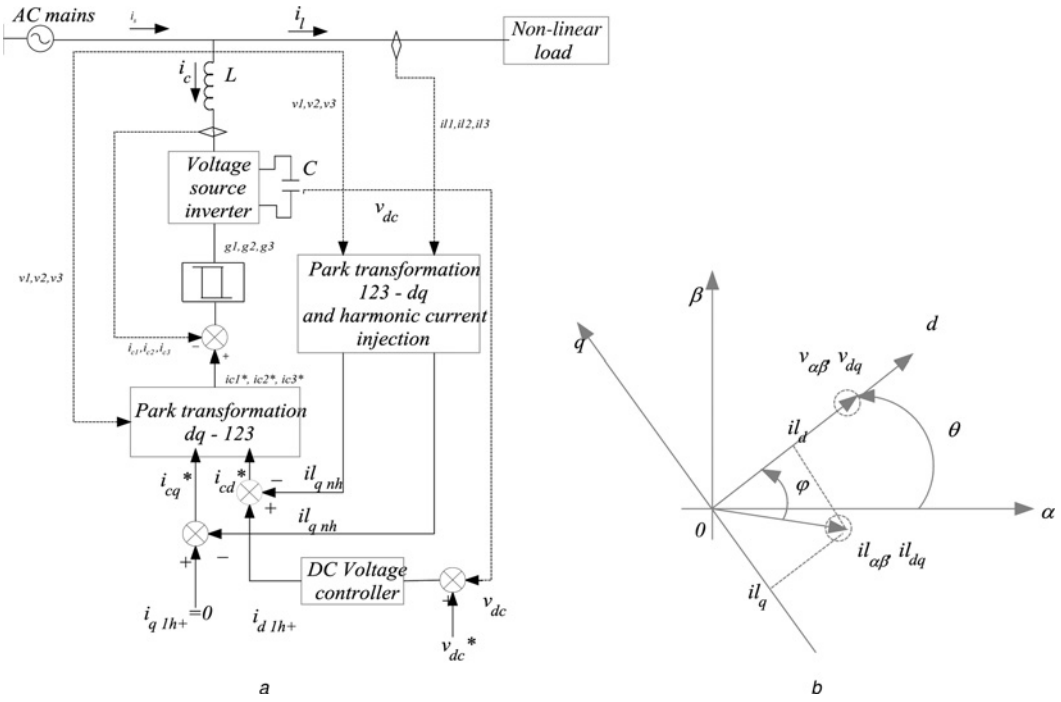

Fig. 2 *i_d–i_q strategy for perfect compensation*

a Active powers filter control circuit
b Voltage and current vectors in stationary and rotating reference frames

In this method reference currents are obtained through instantaneous active and reactive currents i_d and i_q of the non-linear load. *dq* load current can be obtained from (5). Two-stage transformations yield a relation between the stationary and rotating reference frame. Fig. 2*b* shows the voltage and current vectors in stationary and rotating reference frames. The transformation angle θ is sensitive to all voltage harmonics and unbalanced voltages; as a result $\mathrm{d}\theta/\mathrm{d}t$ may not be constant. Arithmetical relations are given in (10) and (6); finally reference currents are obtained from (7). One of the major advantages of this approach is angle θ, which is calculated directly from the main voltage

$$\begin{bmatrix} i_d \\ i_q \end{bmatrix} = \frac{1}{\sqrt{v_\alpha^2 + v_\beta^2}} \begin{bmatrix} v_\alpha & v_\beta \\ -v_\beta & v_\alpha \end{bmatrix} \begin{bmatrix} i_\alpha \\ i_\beta \end{bmatrix} \tag{5}$$

$$\begin{bmatrix} i_d \\ i_q \end{bmatrix} = \begin{bmatrix} \cos\theta & \sin\theta \\ -\sin\theta & \cos\theta \end{bmatrix} \begin{bmatrix} i_\alpha \\ i_\beta \end{bmatrix}, \quad \theta = \tan^{-1}\left(\frac{v_\alpha}{v_\beta}\right) \tag{6}$$

$$\begin{bmatrix} ic_\alpha \\ ic_\beta \end{bmatrix} = \frac{1}{\sqrt{v_\alpha^2 + v_\beta^2}} \begin{bmatrix} v_\alpha & -v_\beta \\ v_\beta & v_\alpha \end{bmatrix} \begin{bmatrix} ic_d \\ ic_q \end{bmatrix} \tag{7}$$

This enables the system to be frequency independent by avoiding the phase-locked loop (PLL) in the control circuit, consequently, synchronising problems with unbalanced and distorted conditions of main voltage are also evaded. Thus, i_d–i_q achieves a large frequency operating limit essentially by the cut-off frequency of the voltage source inverter (VSI). From the control diagram of the shunt active filter, load currents i_d and i_q are obtained from Park transformation, then they are allowed to pass through the high-pass filter to eliminate the DC components in the non-linear load currents. The filters used in the circuit are Butterworth type, to reduce the influence of a high-pass filter. An alternative high-pass filter (AHPF) can be used in the circuit, which can be obtained through the low-pass filter (LPF) of same order and cut-off frequency. This can be achieved simply from the difference of the input signal and filtered one. The Butterworth filter used in harmonic injecting circuit has a cut-off frequency equal to one-half of the main frequency ($f_c = f/2$), with this, a small phase shift in harmonics and sufficiently high-transient response can be obtained.

3 Adaptive hysteresis current control

The hysteresis-band current control technique has been confirmed to be the most suitable for all the applications of current controlled VSIs in IPM machines, grid connected systems and active power filters. The hysteresis-band current control is characterised by unconditioned stability, very fast response and good accuracy. On the other hand, the basic hysteresis technique also exhibits several undesirable features, such as asymmetrical switching frequency that causes acoustic noise and difficulty in designing input filters. The conventional hysteresis-band current control idea used for the control of active power filter line current is demonstrated in Figs. 3*a* and *b*. It is composed of a hysteresis around the reference line current. The reference line current of the active power filter is referred to as i_a^* and actual line current of the active power filter is referred to as i_a. The hysteresis-band current controller decides the switching pattern of the active power filter [6]. However, such switching results in high switching loss in the system. To evade this problem an adaptive band is incorporated in the system [11]. This facilitates the hysteresis band to modulate with the system parameters to maintain the modulating frequency to nearly constant. Details of adaptive hysteresis current control are illustrated in Fig. 3*c*. The logic of the adaptive hysteresis band is given in (10). An in-depth assessment of logic with mathematical expression can be found in [7]. To facilitate

doi: 10.1049/iet-pel.2011.0371

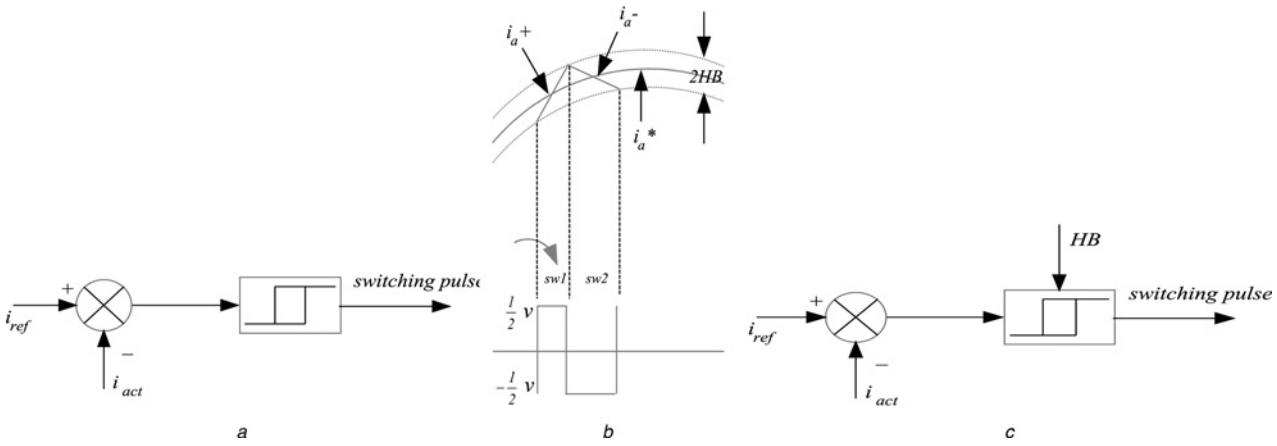

Fig. 3 *Conventional hysteresis-band current control idea for the control of active power filter line current*

a Details of voltage and current wave with hysteresis-band current controller
b Details of hysteresis band current controller
c Details of adaptive hysteresis current control

such prospects in the system unequal switching is evaded

$$\mathrm{HB} = \frac{V_{\mathrm{DC}}}{6 f_{\mathrm{m}} L_{\mathrm{f}}}\left(1 - 9L_{\mathrm{f}}^2\left(\frac{V_{\mathrm{s}}(t)}{L_{\mathrm{f}}} + \frac{\mathrm{d}i_{\mathrm{fa}}^*}{\mathrm{d}t}\right)\right), \quad j = 1, 2, 3 \qquad (8)$$

The above equation expresses the adaptive hysteresis logic, where f_{m} is the modulation frequency, i_{fa}^* is the source reference current and $\mathrm{d}i_{\mathrm{fa}}^*/\mathrm{d}t$ represents its slope, L_{f} is the decoupling inductance of the active power filter, V_{DC} is the DC bus voltage and $V_{\mathrm{s}}(t)$ is the supply voltage.

4 Conventional DC voltage regulation with PI controller

DC voltage optimisation is one of the key aspects in harmonics compensation, SAPF performance is entirely dependent on capacitor voltage. In fact, it influences reference current generation. Although the controller is quite good in generating reference currents, however, in practice with linear controller (PI), information on the DC side is misleading. Details of the harmonic injection circuit and the voltage regulator are demonstrated in Figs. 4*a* and *b*. Inputs to the PI controller are changed in DC-link voltage (V_{DC}) and reference voltage (V_{DC}^*). By regulating the first harmonic active current of positive sequence i_{dlh}^+ the active power flow in the VSI and thus the capacitor voltage V_{DC} can be controlled. In a similar fashion reactive power flow is controlled by i_{qlh}^+. On the contrary, the primary end of the active power filters is simply the exclusion of the harmonics caused by non-linear loads hence the current i_{qlh}^+ is always set to zero.

The linearised model of the system is obtained by neglecting the losses in the inductances and switching devices, that is, assuming that the active power flow from the mains to the VSI is equal to the active power in the DC side and it is demonstrated in Fig. 4*b*; where $C(s)$ and $G(s)$ are the transfer functions of the PI controller and VSI, respectively. The DC voltage regulator is synthesised by assuming a unitary transfer function for VSI and without disturbance, that is, the absence of extra load at the capacitor. Under these findings, a closed-loop transfer function can be expressed as

$$\frac{\Delta V_{\mathrm{DC}}}{\Delta V_{\mathrm{DC}}^*} = \frac{(k_{\mathrm{p}} u_{\mathrm{d}}/C v_{\mathrm{DC}}^0)(s + (k_{\mathrm{i}}/k_{\mathrm{p}}))}{s^2 + (u_{\mathrm{d}}/C v_{\mathrm{DC}}^0)((ic_d^0/v_{\mathrm{DC}}^0) + k_{\mathrm{p}})s + (k_{\mathrm{i}} u_{\mathrm{d}}/C v_{\mathrm{DC}}^0)} \qquad (9)$$

k_{p} and k_{i} are the proportional and integral gains of the PI controller. C is the DC-link capacitor, V_{DC}^0 and i_{DC}^0 are the capacitor voltage and current at linearising conditions. u_{d} is the mains voltage. However, by controlling the gains of k_{p} and k_{i}, DC-link optimisation can be achieved effectively.

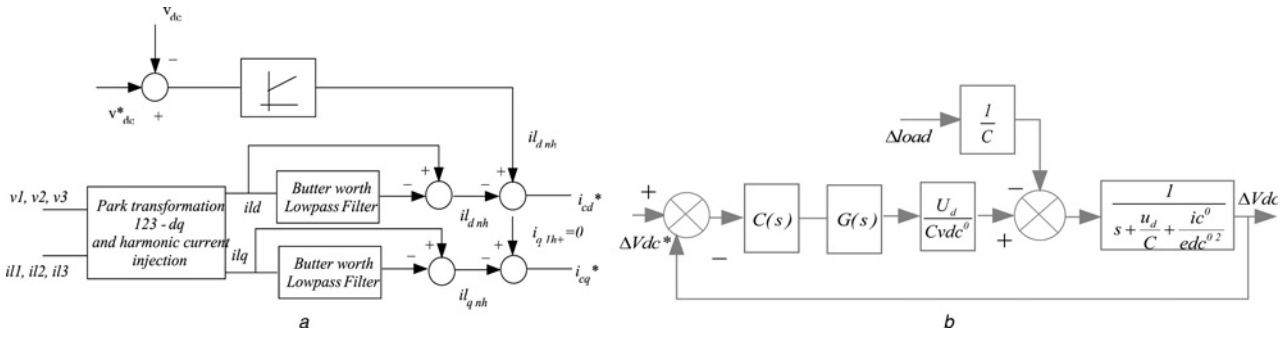

Fig. 4 *Details of harmonic injection circuit and voltage regulator*

a Park transformation and harmonic current injection circuit
b Details of DC voltage regulator

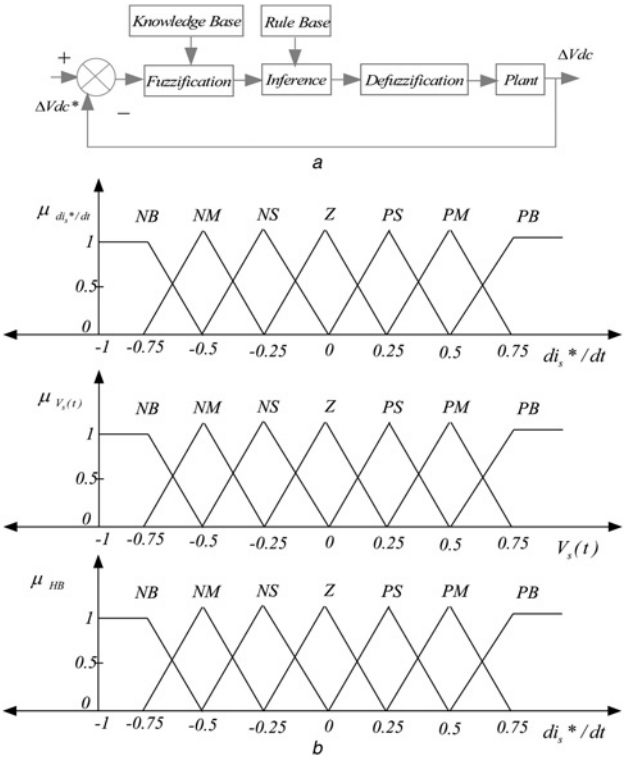

Fig. 5 *DC optimisation with fuzzy approach*

a Details of block diagram of FLC
b Membership shapes of I/O fuzzy sets and assignment of the control rules in the error phase plane

5 Proposed DC voltage regulation with fuzzy controller

The concept of fuzzy logic was introduced in the year 1965, since then fuzzy logic has become a powerful computation paradigm. Numerous fuzzy control applications have been observed in the literature. In this article such a powerful computational algorithm is used for DC voltage optimisation. In fact, compared with the PI controller, fuzzy control is basically an adaptive and non-linear controller, that gives robust performance for a linear or non-linear plant with parameter variations. However, for obvious reasons, fuzzy stands as the best adaptive control among all controllers. There are essentially two methods for implementation of fuzzy control. The first one involves rigorous mathematical computation for fuzzification, evaluation of control rules and defuzzification in real time. The other one is with C program with FL tool box in Matlab environment. In this case we follow the first method. Fig. 5*a* demonstrates DC optimisation with fuzzy approach. In brief, fuzzy logic uses fuzzy set theory, in which the variable is a member of one or more sets, with a specified degree of membership. A common fuzzy logic controller (FLC) mainly consists of three blocks, namely fuzzification, inference and defuzzification. An in-depth assessment of the above blocks can be found in [9]. To be specific, fuzzy logic is adopted only for error optimisation. Fig. 5*b* provides information about the error component optimisation paradigm.

5.1 Design of fuzzy logic membership functions

An important design aspect in FLC is rule base and shape of fuzzy sets. The shape of a fuzzy set affects how well a fuzzy system of if–then rules approximates a function. Triangles have been the most appropriate and popular if-part shape of approximating a non-linear function. The authors reported in [12, 14, 15] have shown that triangular membership function is most economical in the sense of the above-mentioned parameters. The foremost things in triangular membership functions are their striking simplicity, solid theoretical basis and ease of computation.

However, development of rules entails a thorough logical understanding with specific process and in the present paradigm the proposed FLC is characterised as follows:

1. 'seven' fuzzy sets for each input and output;
2. 'triangular' membership functions for each input and output;
3. fuzzification using continuous universe of discourse;
4. implication using 'min' operator;
5. 'inference' mechanism based on fuzzy implication;
6. defuzzification using the 'centriod' method.

Membership functions and rules are obtained by understanding the APF behaviour. On the other hand, Fig. 10 provides the details of the membership functions of the I/O fuzzy set and assessment of control rules and two inputs are considered as triangular membership functions and output is taken as a constant membership function. On the other hand, the interpretations are evidently demonstrated in Fig. 10, by following a systematic procedure, a stable and optimised error-free approach can be found. Table 1 provides the details of 49 rules to carry out optimum control action and each rule expresses an operating condition in the system. In common, 49 rules can guarantee acceptable and optimum control.

Table 1 Fuzzy decision table

V_{DC}	$V_{DC\text{-}ref}$						
	NB	NM	NS	Z	PS	PM	PB
NB	NB	NB	NB	NB	NM	NS	Z
NM	NB	NB	NB	NM	NS	Z	PS
NS	NB	NB	NM	NS	Z	PS	PM
Z	NB	NM	NS	Z	PS	PM	PB
PS	NM	NS	Z	PS	PM	PB	PB
PM	NS	Z	PS	PM	PB	PB	PB
PB	Z	PS	PM	PB	PB	PB	PB

6 System performance with a real-time digital simulator

6.1 Real-time digital simulator

The RTDS allows developers to accurately and efficiently simulate electrical power systems and their ideas to improve them. The RTDS [13] operates in real- time, therefore not only allowing simulation of the power system, but also making it possible to test physical protection and the control equipment. This gives developers the means to prove their ideas, prototypes and final products in a realistic environment. The RTDS is a fully digital power system simulator capable of continuous real-time operation. It performs electromagnetic transient power system simulations with a typical time step of 50 μs utilising a combination of custom software and hardware. The proprietary operating system used by the RTDS guarantees 'Hard real time' during all simulations. It is an ideal tool for the design, development

doi: 10.1049/iet-pel.2011.0371

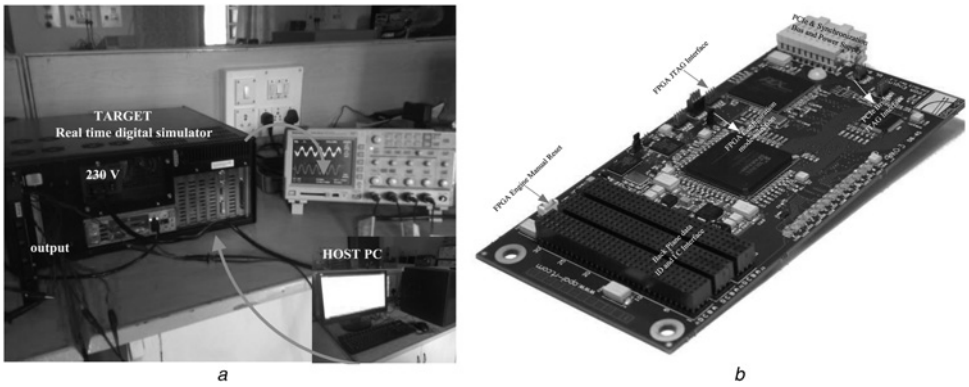

Fig. 6 *Typical hardware configurations*

a Details of RTDS hardware set-up
b OP5142 layout and connectors

and testing of power system protection and control schemes. With a large capacity for both digital and analogue signal exchange (through numerous dedicated, high-speed I/O ports) physical protection and control devices are connected to the simulator to interact with the simulated power system.

6.2 Simulator hardware

The real-time digital simulation hardware used in the implementation of the RTDS is modular, hence making it possible to size the processing power to the simulation

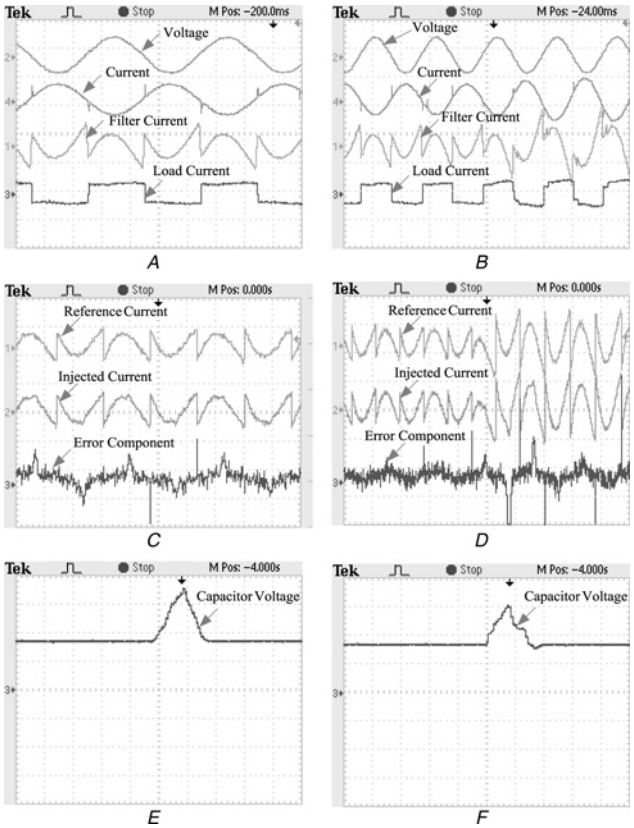

Fig. 7 *Performance of APF with PI controller*

A Performance of system under steady state condition: (a) supply voltage, (b) source current (scale 30 A/div), (c) filter current (scale 20 A/div), (d) load current (scale 20 A/div)
B Performance of system under step change in load: (a) supply voltage, (b) source current (scale 30 A/div), (c) filter current (scale 20 A/div), (d) load current (scale 20 A/div)
C Performance of system under steady state condition: (a) reference current (30 A/div), (b) injected current (scale 30 A/div), (c) error in current component (scale 20 A/div)
D Performance of system under step change in load: (a) reference current (30 A/div), (b) injected current (scale 30 A/div), (c) error in current component (scale 20 A/div)
E and *F* Details of capacitor variations

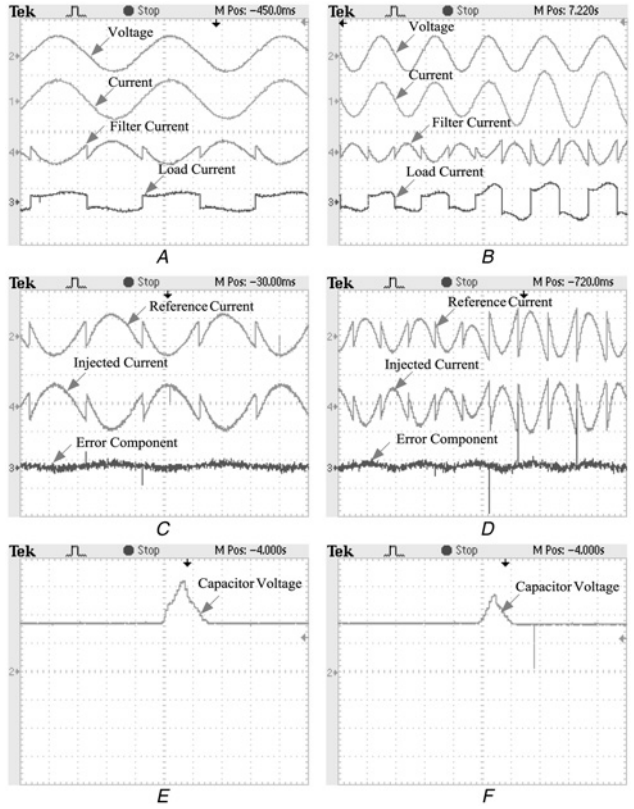

Fig. 8 *Performance of APF fuzzy controller*

A Performance of system under steady state condition: (a) supply voltage, (b) source current (scale 30 A/div), (c) filter current (scale 20 A/div), (d) load current (scale 20 A/div)
B Performance of system under step change in load: (a) supply voltage, (b) source current (scale 30 A/div), (c) filter current (scale 20 A/div), (d) load current (scale 20 A/div)
C Performance of system under steady state condition: (a) reference current (30 A/div), (b) injected current (scale 30 A/div), (c) error in current component (scale 20 A/div)
D Performance of system under step change in load: (a) reference current (30 A/div), (b) injected current (scale 30 A/div), (c) error in current component (scale 20 A/div)
E and *F* Details of capacitor variations

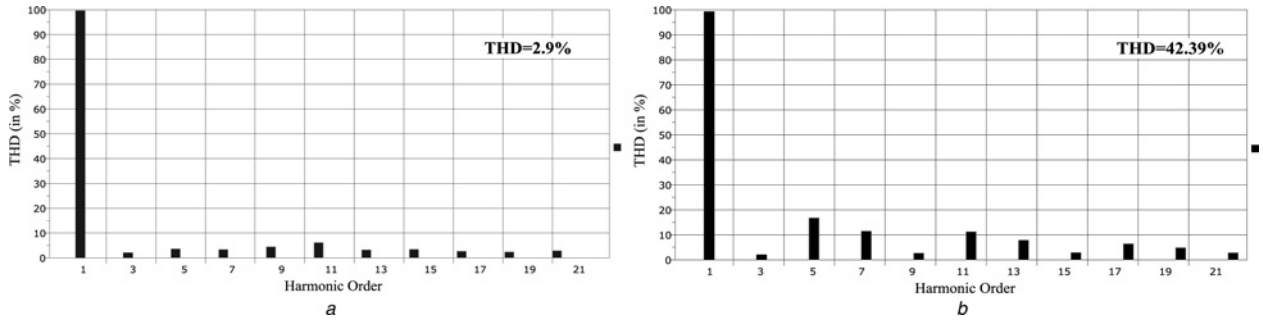

Fig. 9 *Information of THD before and after compensation with PI controller*

a Harmonic spectrum of source current with conventional adaptive hysteresis-band controller
b Harmonic spectrum of the non-linear load current

tasks at hand. Fig. 6 demonstrates typical hardware configurations. The OP5142 (Fig. 6*b*) is one of the key building blocks in the modular OP5000 I/O system from Opal-RT technologies. It allows the incorporation of FPGA technologies in RT-LAB simulation clusters for distributed execution of hardware description language (HDL) functions and high-speed, high-density digital I/O in real-time models. Based on the highest density Xilinx Spartan-3 FPGA, the OP5142 can be attached to the backplane of an I/O module of either a Wanda 3U- or Wanda 4U-based Opal-RT simulation system. It communicates with the target PC via a PCI-Express ultra-low-latency real-time bus interface. As can be seen, the simulator can take on several forms including a new portable version, which can easily be transported to a power plant or substation for on-site pre-commissioning tests. Each rack of simulation hardware contains both processing and communication modules. The mathematical computations for individual power system components and for network equations are performed using one of the two different processor modules.

6.3 System performance with the PI controller

The real-time digital verifications are depicted in Fig. 7. The experimentation has been carried out at switching frequency 10 kHz. The non-linear load and the APF are connected at $t = 0$ s. For obvious reasons the bridge load generates harmonics and APF capable of compensating effectively by injecting non-sinusoidal harmonics at the point of common coupling. Fig. 7*A* provides information about source voltage, source current, filter current and load current (from top to bottom) under steady-state conditions with balanced supply voltage. Furthermore, to study the performance of the APF under transient conditions, a step change in load is created at $t = 0.5$ s. Fig. 7*B* provides the details of, source voltage, source current, filter current and load current (from top to bottom) under transient conditions with balanced supply voltage. Although the APF succeeded in compensating harmonic currents, however notches are observed in the source current. The main reason behind the notches is that the controller failed to track the information correctly and thereby the APF fails to compensate completely. On the other hand, Figs. 7*C* and *D* provide information about the error components. These error components decide the controller performance. More the error, poorer the compensation. From Fig. 7*C* reference currents and injected currents are taken into account and then the error component is predicted. Observing the performance, the error component had large ripples and this

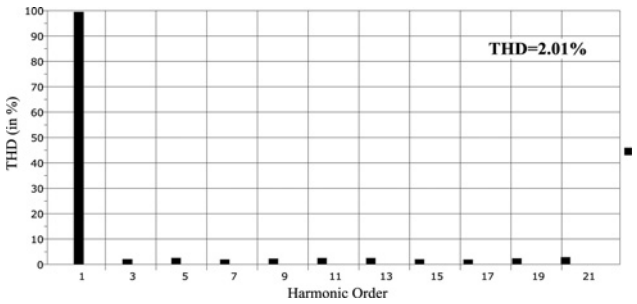

Fig. 10 *Harmonic spectrum of source current with adaptive fuzzy hysteresis current controller*

is all because of the PI controller. Furthermore, Figs. 7*E* and *F* provide information about DC-link voltage with different capacitors. In this scenario, the capacitances used are 3 and 5 μF. With a large capacitance, the DC-link voltage takes a long time to settle down and the ripple content drastically reduces. As the capacitance reduces the ripple content increases predominantly. Furthermore, Figs. 9*a* and *b* provide information about THD before and after compensation, where it is about 42.3 and 2.9% of the load and source currents, respectively, with the PI controller.

6.4 System performance with fuzzy controller

Fig. 8 highlights the performance of the APF with the fuzzy controller. As before, the experimentation is carried out at $t = 0$ s. Fig. 8*A* provides the details of source voltage, source current, filter current and load current under balanced supply conditions. Note that the APF provides an outstanding compensation. The source current is quite clean in nature without any ripples. Fig. 8*B* provides the performance of the APF under a transient event. Same as before, source voltage, source current, filter current and load current are demonstrated from top to bottom order. It is to be noted that the source current waveform is fairly good and notches in the waveform are eliminated. On the other hand, Figs. 8*C* and *D* provide information about the error component, which is predicted through reference and injected currents. Note that the error component is entirely nullified and this completely defines the potential and the performance of the fuzzy controller. The error component waveforms presented in Fig. 8*D* with the PI controller are quite a disaster and this error component is still higher under transient conditions in the PI controller, but such prospects are completely nullified with the proposed

doi: 10.1049/iet-pel.2011.0371

approach. Figs. 8*E* and *F* provide the details of DC-link voltage with different capacitance; however, variations in DC voltage are quite satisfactory. The system is able to settle down within a minimum amount of time, both in the transient and the steady-state conditions; whereas the same phenomena are not observed in the PI controller. However, comparing waveforms, which are reported in Figs. 8*E* and 7*E*, signifies excellent performance with the proposed controller in terms of DC optimisation. Fig. 10 demonstrates THD information with fuzzy controller. THD is around 40 and 2% in the load and the source currents, respectively. Thus, with adaptive fuzzy hysteresis control, system performance is improved dramatically.

7 Conclusion and discussion

This paper has proposed an adaptive fuzzy hysteresis control shunt active filter. The proposed filter, which compensates for the current harmonics generated by the contaminating load, was verified using the RTDS. It has been demonstrated that the filter responds very effectively under steady-state and transient conditions. To verify the effective nature of the controllers, error component waveforms are incorporated, which signifies the performance of both the PI and the fuzzy controllers. Reduction of harmonic content on source current waveforms and minute DC-link voltage variations signify the improvement of APF compensations. Thus, with the proposed algorithm and by taking advantage of the adaptive hysteresis band a novel shunt active filter is developed.

8 References

1 Rudnick, H., Dixon, J., Morán, L.: 'Delivering clean and pure power', *IEEE Power Energy Mag.*, 2003, **1**, (5), pp. 32–40

2 Owen, E.L.: 'A history of harmonics in power systems', *IEEE Ind. Appl. Mag.*, 1998, **4**, (1), pp. 6–12

3 Bhattacharya, A., Chakraborty, C., Bhattacharya, S.: 'Shunt compensation', *IEEE Trans. Ind. Electron. Mag.*, 2009, **3**, (3), pp. 38–49

4 Buso, S., Malesani, L., Mattavelli, P.: 'Comparison of current control techniques for active filter applications', *IEEE Trans. Ind. Electron.*, 1998, **45**, (5), pp. 722–729

5 Shuai, Z., Luo, A., Tu, C., Liu, D.: 'New control method of injection-type hybrid active power filter', *IET Power Electron.*, 2011, **4**, (9), pp. 1051–1057

6 Holh, I.: 'Pulse width modulation – a survey', *IEEE Trans. Ind. Electron.*, 1999, **39**, (5), pp. 410–420

7 Bose, B.K.: 'An adaptive hysteresis-band current control technique of a voltage-fed PWM inverter for machine drives system', *IEEE Trans. Ind. Electron.*, 1990, **37**, (5), pp. 402–408

8 kale, M., Ozdemir, E.: 'An adaptive hysteresis band current controller for shunt active power filter', *Elsevier Electr. Power Syst. Res.*, 2005, **73**, pp. 113–119

9 Mekri, F., Mazari, B., Machmoum, M.: 'Control and optimization of shunt active power filter parameters by fuzzy logic', *IEEE Electr. Comput. Eng.*, 2006, **31**, (3), pp. 127–134

10 Soares, V., Verdelho, P.: 'An instantaneous active and reactive current component method for active filters', *IEEE Trans. Power Electron.*, 2000, **15**, (4), pp. 660–669

11 Rahman, K.M., Rezwan Khan, M., Choudhury, M.A., Rahman, M.A.: 'Variable-band hysteresis current controllers for PWM voltage-source inverters', *IEEE Trans. Power Electron.*, 1997, **12**, (6), pp. 964–970

12 Oh, D.S., Youn, M.J.: 'Automated adaptive hysteresis current control technique for a voltage-fed PWM inverter', *IET Electron. Lett.*, 1990, **4**, (24), pp. 2044–2046

13 Xiao, P., Venayagamoorthy, G.K., Corzine, K.A.: 'Seven-level shunt active filter for high power drive systems', *IEEE Trans. Power Electron.*, 2009, **24**, (1), pp. 6–13

14 Teke, A., Bayindir, K., Tumay, M.: 'Fast sag/swell detection method for fuzzy logic controlled dynamic voltage restorer', *IET Gener. Transm. Distrib.*, 2009, **4**, (1), pp. 1–12

15 Yi, S.Y., Chung, M.J.: 'Robustness of fuzzy logic control for an uncertain dynamic system', *IEEE Trans. Fuzzy Syst.*, 1998, **6**, (2), pp. 216–225